



ENGINEERING MATHEMATICS
AND COMPUTING LAB



UNIVERSITÄT
HEIDELBERG
ZUKUNFT
SEIT 1386

Comparison of mesh-adaptation criteria for an idealized tropical cyclone problem

Martin Baumann, Teresa Beck, Vincent Heuveline, Sarah Jones, Leonhard Scheck

Preprint No. 2015-01

Preprint Series of the Engineering Mathematics and Computing Lab (EMCL)





Preprint Series of the Engineering Mathematics and Computing Lab (EMCL)

ISSN 2191-0693

Preprint No. 2015-01

The EMCL Preprint Series contains publications that were accepted for the Preprint Series of the EMCL. Until April 30, 2013, it was published under the roof of the Karlsruhe Institute of Technology (KIT). As from May 01, 2013, it is published under the roof of Heidelberg University.

A list of all EMCL Preprints is available via Open Journal System (OJS) on <http://archiv.ub.uni-heidelberg.de/ojs/index.php/emcl-pp/>

For questions, please email to

info.at.emcl-preprint@uni-heidelberg.de

or directly apply to the below-listed corresponding author.

Affiliation of the Authors

Martin Baumann¹, Teresa Beck^{1,2,a}, Vincent Heuveline¹, Sarah Jones³, Leonhard Scheck^{1,4}

¹*Engineering Mathematics and Computing Lab, Interdisciplinary Center for Scientific Computing, Heidelberg, Germany*

²*Institute for Meteorology and Climate Research, Karlsruhe Institute of Technology, Karlsruhe, Germany*

³*Deutscher Wetterdienst, Offenbach, Germany*

⁴*Hans-Ertel-Centre for Weather Research, Ludwig-Maximilians-Universität München, Germany*

^a*Corresponding Author: Teresa Beck, Teresa.Beck@iwr.uni-heidelberg.de*

Impressum

Heidelberg University

Interdisciplinary Center for Scientific Computing (IWR)

Engineering Mathematics and Computing Lab (EMCL)

Speyerer Str. 6,
69115 Heidelberg
Germany

Published on the Internet under the following Creative Commons License:

<http://creativecommons.org/licenses/by-nc-nd/3.0/de> .



www.emcl.iwr.uni-heidelberg.de

Comparison of mesh-adaptation criteria for an idealized tropical cyclone problem

Martin Baumann, Teresa Beck, Vincent Heuveline, Sarah Jones, Leonhard Scheck

July 27, 2015

Abstract

The development and motion of tropical cyclones is influenced by processes on a wide range of scales. Adaptive meshes are a promising way to reduce the computational costs of numerical simulations for such multiscale problems. Mesh adaptation can be controlled by various criteria for which cell-wise indicators are typically introduced. We analyze indicators based on a posteriori error estimators, goal-oriented error estimators, and physical criteria. To compare these different approaches, we propose indicators for physical quantities formulated in a way that allows us to apply the same mesh adaptation strategy to all cases. As a benchmark problem we investigate the interaction of two tropical cyclones in an idealized framework. On adaptive meshes, the track prediction error could be reduced up to two orders of magnitude compared to uniform meshes. We describe the costs for the computational evaluation of the investigated indicators and discuss the efficiency of the resulting adaptive methods.

1 Introduction

In numerical weather prediction and climate modeling, dynamical processes on a wide range of spatial and temporal scales need to be considered. A higher resolution of the discretization mesh allows for a better representation of the state of the atmosphere but leads to increased computational costs at the same time. One way to discretize phenomena with multiscale characteristics efficiently is given by using a varying mesh resolution, as the computational effort can often be reduced considerably by using a high-resolution grid only in the parts of the domain where an accurate representation of the solution is necessary. Adjustable mesh resolution can be accomplished e.g. by refining or coarsening mesh cells (h-adaptivity), moving grid points (r-adaptivity) or nesting techniques. For an overview of adaptive methods for geoscientific application, see for example Jablonowski [2004] and Behrens [2006].

All these approaches require a strategy to control the structure of the mesh for a given scenario. From a mathematical point of view, the idea of adapting a mesh arises from the framework of error estimation and aims at reducing the total error by refining cells with high local error contributions [see Ainsworth and Oden, 2000]. In that context it is well-motivated to characterize an *optimal mesh* by an equilibration of error contributions [cf. Babuka and Rheinboldt, 1978, Eriksson and Johnson, 1991, Huang and Russell, 2011]. However, in meteorological applications one often uses heuristic criteria, for instance related to orography or specific physical properties of the solution to control the adaptation process [cf. Jablonowski, 2004]. In most of these cases, no definition of an *optimal mesh* can be deduced.

In practice, it is not clear which criterion leads to the most efficient adaptive method that achieves the best balance of costs and quality of the resulting numerical simulation in application depending measures. The identification of an appropriate adaptation criterion therefore is an important task. If too many elements are refined, the approximated solution improves, but the method may lose efficiency since the increase in computing time might exceed the increase in accuracy. If too few or the wrong elements are refined, the improvement of the solution may not be sufficient to justify the computational overhead for the refinement. At the *Newton Institute Scoping Meeting on Multiscale Modeling Of The*

Atmosphere And Ocean in 2009, adaptation criteria have been pointed out as one of the outstanding issues concerning adaptivity [cf. Weller et al., 2010]. Within Newton Institute’s program *Multiscale Numerics for the Atmosphere and Ocean* in 2012, adaptation criteria again have been one of the major issues.

In this article, we investigate the efficiency of static grid adaptation (i.e. the mesh is not being changed during the simulation) based on different adaptation criteria. As a test case, we consider the interaction of two tropical cyclones (TCs) in a barotropic framework. Since the development of the two storms in numerical simulations can be affected strongly by too coarse grid resolution, this scenario is well suited as a benchmark problem for adaptive mesh methods. The investigations in this article supplement the research in Bauer et al. [2013] and Baumann et al. [2014], where exclusively goal-oriented estimators are investigated for the same scenario. Here, we investigate further, computationally cheaper indicators.

The mesh adaptation is steered by indicators based on a posteriori estimators for the error in global norms, goal-oriented error estimators, and physically motivated criteria. The indicators are being compared with respect to their efficiency, defined as the relation of numerical costs and quality of the solution. We use the same adaptation strategy for every criterion, which aims at an equidistribution of indicator values over the cells of a mesh. This strategy presumes that the indicator values depend on the mesh width. The indicators based on a posteriori error estimations fulfill this property, whereas for the physical indicators a dependency on the mesh width has to be added explicitly by construction.

This article is structured as follows: In Sect. 2 we describe the model equations and their discretization in terms of finite elements. A description of the binary TC interaction scenario follows in Sect. 3. In Sect. 4, the different adaptation criteria are formulated and discussed. These criteria are applied to the TC scenario to control the mesh adaptation process. In Sect. 5 we present the numerical results together with the resulting adapted meshes and discuss the efficiency of each criterion. Finally, Sect. 6 contains a summary and conclusions.

2 Barotropic model and discretization

2.1 Continuous model equations

We use a barotropic model corresponding to the incompressible Navier-Stokes equations in two dimensions, which have the form

$$\begin{cases} \partial_t u + (u \cdot \nabla)u - \nu \Delta u + \nabla p = 0, & \text{in } \Omega_t, \\ \nabla \cdot u = 0, & \text{in } \Omega_t, \\ u|_{t=0} = u_0, & \text{in } \Omega, \end{cases} \quad (1)$$

where $\Omega_t := (0, T) \times \Omega$ with the periodic spatial domain being $\Omega = [0, L_1] \times [0, L_2] \subset \mathbb{R}^2$. We denote the velocity vector field by $u : \Omega_t \rightarrow \mathbb{R}^2$ and the pressure field by $p : \Omega_t \rightarrow \mathbb{R}$. Both fulfill the periodicity conditions

$$\Phi(t, x) = \Phi(t, x + e_1 \cdot L_1) = \Phi(t, x + e_2 \cdot L_2), \quad (2)$$

for any $(t, x) \in \Omega_t$ with the unit vectors $e_1 := (1, 0)^T$ and $e_2 := (0, 1)^T$ and horizontal periodicities of lengths $L_1, L_2 > 0$ in units of km.

Since we subsequently want to use a finite element method based on a Galerkin projection, we consider in the following a variational formulation of problem (1). A common mixed form formulation can be stated as described in Gunzburger [1989] and Quarteroni and Valli [1994]. Let the space of the velocity functions be defined as the periodic Sobolev space $V := H_p^1(\Omega)^2$ [for details see Temam, 1995] and the pressure space be defined as $Q := L_0^2(\Omega) := \{p \in L^2(\Omega) \mid \int_{\Omega} p \, dx = 0\}$. For a given initial velocity field $u_0 \in V$, the problem reads: Find $u(t) \in V$ and $p(t) \in Q$ such that for almost every $t \in (0, T)$

$$\begin{cases} d_t(u(t), \varphi) + ((u(t) \cdot \nabla)u(t), \varphi) \\ + \nu(\nabla u(t), \nabla \varphi) - (p(t), \nabla \cdot \varphi) = 0, \\ (\nabla \cdot u(t), \psi) = 0, \\ u|_{t=0} = u_0 \end{cases} \quad (3)$$

holds for any $\varphi \in V$ and any $\psi \in Q$, where $(a, b) := \int_{\Omega} a \cdot b \, dx$. Results on the existence and uniqueness of variational formulations of the Navier-Stokes problem are discussed in Temam [1995].

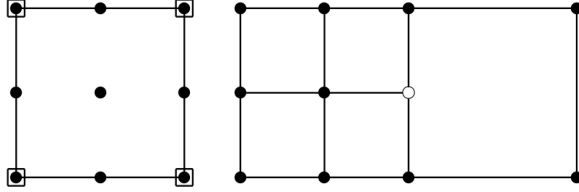


Figure 1: Left: Nodal points of the Taylor-Hood element, i.e. black dots for the bi-quadratic velocity and white boxes for the bi-linear pressure. Right: Cell neighboring a patch consisting of four refined cells with highlighted *hanging node*.

2.2 Discretization in space and time

For the finite element discretization in space, we use a triangulation \mathcal{T}_h of the domain Ω consisting of quadratic cells. We apply a finite element discretization using Taylor-Hood elements that cell-wisely consist of bi-quadratic velocity functions and bi-linear pressure functions (see left panel of Fig. 1), both globally continuous. This type of element is known to be inf-sup stable [cf. Girault and Raviart, 1986]. To guarantee global continuity of discrete functions in case of adapted meshes, we require an additional 1-irregularity condition of the mesh, i.e. on each edge of any cell there may be at most one hanging node of a neighboring cell (see right panel of Fig. 1). On such meshes, global continuity of solutions can easily be achieved by an interpolation condition [see e.g. Heuveline and Rannacher, 2003, Heuveline and Schieweck, 2007]. By this triangulation and finite elements, the discrete function spaces $V_h \subset V$ and $Q_h \subset Q$ are defined.

For the discretization in time, we chose a uniform partitioning $0 =: t_0 < t_1 < \dots < t_N := T$ of the interval $(0, T)$ consisting of $N = 1152$ periods of $\Delta t = t_i - t_{i-1} = 300$ s duration. We apply the Crank-Nicolson (CN) scheme to step through the time intervals and solve the resulting nonlinear problems using Newton's method. The discrete problem on the i -th time-interval (t_i, t_{i-1}) has the form: Find $(u_h^{(i)}, p_h^{(i)}) \in V_h \times Q_h$ such that for any $\varphi \in V_h$ and $\psi \in Q_h$ holds

$$\left\{ \begin{array}{l} (u_h^{(i)}, \varphi) + \Delta t [((u_h^{(i)} \cdot \nabla) u_h^{(i)}, \varphi) + \nu (\nabla u_h^{(i)}, \nabla \varphi)] \\ + \Delta t [((u_h^{(i-1)} \cdot \nabla) u_h^{(i-1)}, \varphi) + \nu (\nabla u_h^{(i-1)}, \nabla \varphi)] \\ - \Delta t (p_h^{(i)}, \nabla \cdot \varphi) - (u_h^{(i-1)}, \varphi) = 0, \\ (\nabla \cdot u_h^{(i)}(t), \psi) = 0. \end{array} \right. \quad (4)$$

For the goal-oriented error estimation that we will investigate later, a differing time-discretization is needed, which leads to discrete solutions that can be interpreted as Galerkin-approximations. In this case, we apply the continuous Galerkin-Petrov cGP(1) method [see Schieweck, 2010] which is a finite element discretization in time. The velocity ansatz functions are piece-wise linear and globally continuous in time. The velocity test functions and the pressure ansatz and test functions are piece-wise constant and may be discontinuous at all t_i . The CN scheme can be interpreted as an inexact variant of the cGP(1) method based on the trapezoidal rule for the time integration. Further details on this discretization variant for the Navier-Stokes equations can be found in Baumann [2012].

For the numerical solution of the discrete variational problem 4, we use the multi-purpose finite element library HiFlow³ [Heuveline, 2010].

3 Benchmark scenario

The interaction of two TCs, which takes place about two times per year [Dong and Neumann, 1983] can reduce the predictability significantly [see Brand, 1970]. Laboratory experiments on the motion of vortices in water have shown that depending on initial conditions different types of interaction are possible, such as merger, mutual orbiting or separation [cf. Fujiwhara, 1923]. Several idealized studies [e.g. Holland and Dietachmayer, 1993, Melander et al., 1988, Ritchie and Holland, 1993] demonstrated that the initial

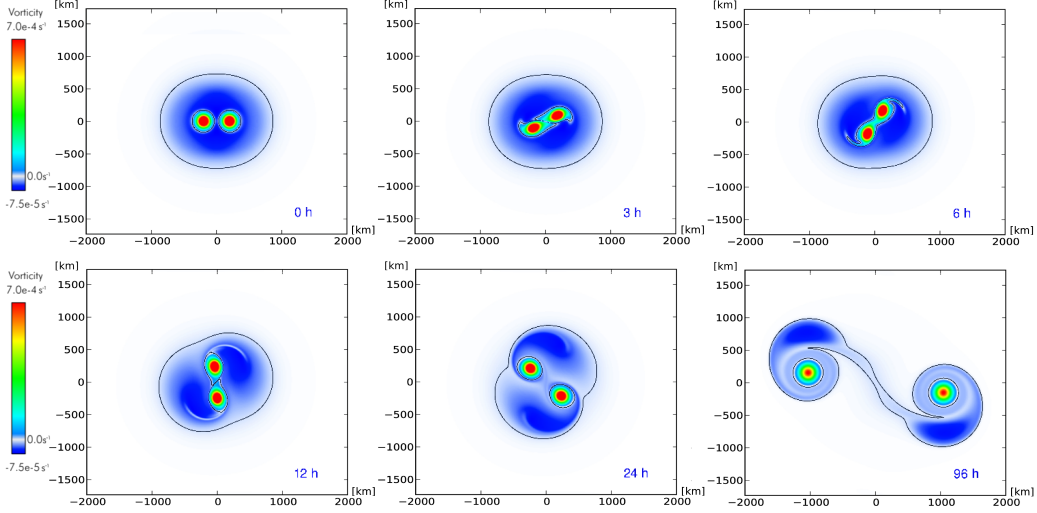


Figure 2: Vorticity distribution of the interacting TCs at $T = 0, 3\text{h}, 6\text{h}, 12\text{h}, 24\text{h},$ and 96h (from top left to bottom right) for the reference run on a uniform grid with 1,327,104 DOFs.

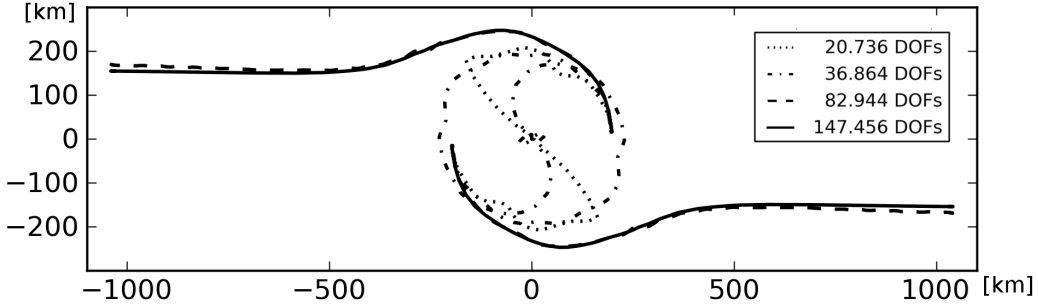


Figure 3: Dependency of storm tracks on the mesh resolution in case of uniform meshes. For high grid resolution the storms separate. For coarse resolution, the storms merge. Grid resolution indicated in degrees of freedom (DOFs).

distance of the vortices plays a key role. If the distance between two identical vortices (the case we will focus on) is initially below a certain critical value, the vortices will eventually merge. For initial distances above the critical value, the vortices will separate. The critical value where this bifurcation takes place is mainly determined by the vortex structure. However, also viscosity has some influence on the critical distance [cf. Ritchie and Holland, 1993].

In numerical experiments mesh width has turned out to be a further influential parameter for the bifurcation. Low mesh resolution causes additional numerical viscosity and thus has a similar effect as increasing the viscosity parameter. On a coarse mesh numerical dissipation can therefore lead to a non-physically merger. Since the dynamics of the two storms is highly sensitive to the grid resolution, this scenario is a challenging benchmark problem for adaptive mesh methods and has already been investigated by Bauer et al. [2013] and Baumann et al. [2014].

3.1 Scenario of two interacting tropical cyclones

In this study, we consider the same test case as in Baumann et al. [2014]. We approximate the dynamics of two interacting TCs using a two-dimensional barotropic model. In order to suppress small-scale noise while keeping the influence on the large-scale flow small, we set the viscosity parameter to $\nu = 5 \cdot 10^3 \text{ m}^2/\text{s}$. We

consider a domain of $\Omega := [-2,000 \text{ km}, 2,000 \text{ km}] \times [-1,732.1 \text{ km}, 1,732.1 \text{ km}]$ with periodic boundaries. Two identical vortices introduced by Smith et al. [1990] are used, which are characterized by a tangential velocity profile

$$u_T(s) := u_0 \frac{s[1 + \frac{6b}{2a}s^4]}{(1 + as^2 + bs^6)^2}, \quad (5)$$

where $a = 0.3398$, $b = 5.377 \cdot 10^{-4}$ and $s = r/r_0$. The reference radius r_0 is chosen to be 100 km and the velocity parameter is $u_0 = 71.521 \text{ m/s}$ which leads to a maximal tangential velocity u_T of 40 m/s. For large distances from the storm center, the vorticity profile is negative, which causes the velocity to decrease faster than with $1/r$, similar to real storms. This idealized representation of a TC has proved to be an adequate simplification to study certain dynamical behaviors of a TC [see e.g. Scheck et al., 2011].

At initial time, the two vortices are located at the positions $(\pm 200 \text{ km}, 0 \text{ km})$. The initial distance of 400 km is only slightly larger than the critical value of about 380 km for this case [see Baumann et al., 2014].

For this setup we performed a high-resolution reference run with 1,327,104 DOFs. The evolution of the vorticity distribution during the simulated time span of 96 hours is shown in Fig. 2. Initially, the interaction is dominated by a mutual orbiting of the two vortices. As discussed in more detail in [Bauer et al., 2013] and [Baumann et al., 2014], the vortices separate after about two days and propagate into opposite directions.

We repeated the reference run on uniform grids with lower resolution and determined the storm tracks. For this purpose, we characterize the storm center by the position of the maximal vorticity and determine it by means of a weighted barycenter of the vorticity in sub-grid accuracy. As visible in Fig. 3, there is a strong dependence of the storm tracks on the resolution. For less than 80,000 DOFs, the storms merge.

4 Adaptation criteria

Grid adaptation usually is an iterative process:

At the begin of each cycle cell-wise refinement indicators are evaluated for the current grid. Subsequently, these indicators are used to adapt the grid according to an adaptation strategy. Once the mesh has been adapted, the problem can be discretized and approximated on the adapted mesh and the iteration proceeds.

In this work, we study different refinement criteria, but always use the same adaptation strategy. We use the *fixed mesh-fraction strategy*, [cf. Becker and Rannacher, 2003], in which a certain percentage of the current number of cells with the highest indicator values is refined in each adaptation cycle. The strategy presumes that refining the mesh will lead to smaller indicator values, which defines the optimal mesh as an equilibration of indicator values. This dependency is an inherent property of mathematical error estimators (assuming small enough cell diameter), but is not in general given for heuristic criteria. We extend this approach for arbitrary adaptation criteria and design respective indicators.

4.1 A posteriori error estimators in global norms

The classical approach of employing a posteriori error estimators for the determination of adaptation indicators is based on the idea of reducing the total error in a global norm by enhancing the resolution in areas with large error contributions to the total error. To evaluate the a posteriori error an explicit knowledge of the continuous solution is not required, as the estimator solely depends on the discrete solution and the definition of the continuous problem. In this section, we introduce two residual a posteriori error estimators [see Babuka and Rheinboldt, 1978] that characterize the spatial discretization error. An estimator variant for the error estimation of Poisson problems and an estimator variant for the stationary Navier Stokes equations are investigated. Both estimator variants are derived for stationary problems and therefore do not fit to the instationary Navier-Stokes problem we are considering. Nevertheless, such estimators can be used to control the mesh adaptation as described e.g. in [Schmich, 2009].

4.1.1 Error estimator for Poisson's problem

On a domain Ω , we consider Poisson's problem with homogeneous Dirichlet boundary conditions and for a given right-hand side denoted by $f : \Omega \rightarrow \mathbb{R}$: Find $u : \Omega \rightarrow \mathbb{R}$ such that

$$\begin{cases} -\Delta u = f, & \text{in } \Omega, \\ u = 0, & \text{on } \partial\Omega \end{cases} \quad (6)$$

holds. We consider a quasi-uniform triangulation \mathcal{T}_h of the domain Ω and seek an approximate solution u_h in a finite dimensional subspace $V_h \subset V := H_0^1(\Omega)$ based on a Galerkin projection of the variational formulation: Find $u_h \in V_h$ such that

$$(\nabla u_h, \nabla \varphi) = (f, \varphi), \quad (7)$$

for all $\varphi \in V$. In terms of an a posteriori error estimator, the discretization error $\|u - u_h\|_{H^1(\Omega)}$ between the finite element solution u_h and the exact solution $u \in V$ of the variational form of problem (6) can be determined. The contributions of any cell $K \in \mathcal{T}_h$ to this error can be characterized in terms of a cell-wise residual R_K and jump terms R_{Γ_K} between neighboring cells. Γ_K represents the set of all cell edges of cell $K \in \mathcal{T}_h$ defined by $\Gamma_K := \{K \cap K' \mid \text{for all } K' \in \mathcal{T}_h, K \neq K'\}$. The cell residual of the discrete solution u_h is defined by

$$R_K(u_h) := (f + \Delta u_h)|_K, \quad (8)$$

for any $K \in \mathcal{T}_h$. The jump term over Γ_K is defined as the sum of the jumps over all edges $e \in \Gamma_K$. The jump over edge e is the flux of the solution through the edge e of the two neighboring cells $K, K' \in \mathcal{T}_h$ with $K \cap K' = e$. The jump is given by

$$R_e(u_h) := (\nabla u_h|_{K' \cap e} - \nabla u_h|_{K \cap e}) \cdot n, \quad (9)$$

for any $e \in \Gamma_K$ where n denotes the outer normal of edge e with respect to element K . An error indication on element K is defined by

$$\eta_K := \left\{ h_K^2 \|R_K\|_{L^2(K)}^2 + \frac{1}{2} \sum_{e \in \Gamma_K} h_e \|R_e\|_{L^2(e)}^2 \right\}^{1/2}, \quad (10)$$

for all $K \in \mathcal{T}_h$, with h_K being the cell diameter and h_e being the length of the edge.¹

An a posteriori error estimator for the $H^1(\Omega)$ -error is given in terms of these indicators by

$$\|u - u_h\|_{H^1(\Omega)} \leq C \left\{ \sum_{K \in \mathcal{T}_h} \eta_K^2 \right\}^{1/2} \quad (11)$$

with some h -independent constant $C > 0$ [cf. Braess, 2007, for example].

4.1.2 Error estimator for the stationary Navier-Stokes problem

The stationary Navier-Stokes equations with periodic boundary conditions and external force f have the form: Find $u \in \Omega \rightarrow \mathbb{R}^2$ and $p \in \Omega \rightarrow \mathbb{R}$ which fulfill a periodicity condition of Eq. (2) such that

$$\begin{cases} -\nu \Delta u + (u \cdot \nabla)u + \nabla p = f, & \text{in } \Omega, \\ \nabla \cdot u = 0, & \text{in } \Omega \end{cases} \quad (12)$$

holds. An approximate solution can be calculated in terms of finite element function spaces $V_h \times Q_h \subset V \times Q$, where the function spaces are the ones introduced for problem (3). As in the previous section, a residual error estimator for a finite element approximation $(u_h, p_h) \in V_h \times Q_h$ can be formulated in terms of cell-wise residuals

$$R_K(u_h) := (f + \nu \Delta u_h - (u_h \cdot \nabla)u_h - \nabla p_h)|_K, \quad (13)$$

¹As we use a triangulation into quadratic cells (as described in Sect. 2.2), a cell's diameter h_K coincides with the length of its edges h_e .

for all $K \in \mathcal{T}_h$ and edge-specific jump terms

$$R_e(u_h) := -\nu(\nabla u_h|_{K' \cap e} - \nabla u_h|_{K \cap e}) \cdot n, \quad (14)$$

similar to Eq. (9). An additional term

$$R_{K,div}(u_h) := (\nabla \cdot u_h)|_K \quad (15)$$

respects for the error contributions corresponding to the divergence-free condition. In terms of these three residuals, the error contribution of cell K can be formulated:

$$\eta_K := \left\{ h_k^2 \|R_K\|_{L^2(K)}^2 + \|R_{K,div}\|_{L^2(K)}^2 + \frac{1}{2} \sum_{e \in \Gamma_K} h_e \|R_e\|_{L^2(e)}^2 \right\}^{1/2}, \quad (16)$$

for any $K \in \mathcal{T}_h$. The error of the solution (u_h, p_h) can be estimated in terms of the cell-wise indicators:

$$\|u - u_h\|_{H^1(\Omega)} + \|p - p_h\|_{L^2(\Omega)} \leq C \left\{ \sum_{K \in \mathcal{T}_h} \eta_K^2 \right\}^{1/2} \quad (17)$$

with some h -independent constant $C > 0$. Further details can be found for example in Verfürth [1989] and in Verfürth and Hackbusch [1990].

4.2 Goal-oriented error estimator

In this section, we introduce a goal-oriented error estimator for the quantification of the discretization errors with respect to a user-specific error measure described by means of a so-called goal-functional. The latter represents a user-defined physical quantity, which is of special interest. In contrast to the a posteriori error estimators defined in Sect. 4.1, which measure only the contribution of each cell to the instantaneous global error, the goal-oriented error estimator takes the time evolution of discretization errors and their future impact on the goal functional into account.

For the scenario under investigation, we focus on the accurate prediction of the two storms' tracks. In case of the barotropic model, the storm center can be identified by the position of the maximum vorticity. Since small vorticity changes can cause arbitrary changes in the position of the maximum vorticity, a corresponding definition would result in a discontinuous functional. However, the *Dual-Weighted Residual* (DWR) framework [Becker and Rannacher, 2003], we will use in the following, requires goal functionals, which are three-times differentiable [cf. Bangerth and Rannacher, 2003]. Therefore, we introduce a functional, as proposed in Baumann et al. [2014], that is correlated with the storm positions. This functional is defined as the integrated vorticity at final time T over both storm cores (denoted by Ω_V), which are the regions where vorticity values are above 50% of the maximum vorticity:

$$J_V(u) := \int_{\Omega_V} \nabla \times u(T, x) \, dx, \quad (18)$$

$$\Omega_V := \{x \in \Omega \mid \nabla \times u(T, x) \geq 0.5 \cdot V_{\max}\},$$

where $V_{\max} := \max_{x \in \Omega} (\nabla \times u(T, x))$.

In addition, we define a second goal-functional aiming at accurately predicting areas of highest kinetic energy. These areas are particularly interesting, as they imply the highest potential of causing great damage. This second functional is defined as integrated kinetic energy over the region where energy values are above 90% of the maximal energy:

$$J_E(u) := \int_{\Omega_E} \|u(T, x)\|^2 \, dx, \quad (19)$$

$$\Omega_E := \{x \in \Omega \mid \|u(T, x)\|^2 \geq 0.9 \cdot E_{\max}\},$$

where $E_{\max} := \max_{x \in \Omega} (|u(T, x)|^2)$. Since the integration domain Ω_E is asymmetric [see Baumann et al., 2014, Sect. 2.2] in contrast to the case of the functional J_V , the structure of correspondingly adapted meshes might be expected to be asymmetric, too. Asymmetric distributions of coarse and fine resolved regions close to storms might cause additional numerical errors which can be investigated considering the second functional.

In the following, we summarize the error estimation approach for a goal-functional denoted by J which can be thought of either being J_E or J_V , for example. For a given approximate solution u_h (related to some mesh) of the continuous (i.e. exact) solution u , the error in the functional J , namely $|J(u) - J(u_h)|$, can be estimated by means of duality arguments. The idea of the DWR method can shortly be presented in terms of an abstract problem, given in variational form: Find $u \in V$ in some Hilbert space V such that

$$\rho(u, \varphi) = 0, \quad (20)$$

for all $\varphi \in V$, where the residual operator $\rho : V \times V \rightarrow \mathbb{R}$ is linear in the second and may be nonlinear in the first argument. For this problem, a Galerkin solution $u_h \in V_h$ in the finite dimensional space $V_h \subset V$ related to some mesh is characterized by

$$\rho(u_h, \varphi) = 0, \quad (21)$$

for any $\varphi \in V_h$. The sensitivity of a goal-functional $J : V \rightarrow \mathbb{R}$ with respect to perturbations of the solution u can be characterized by means of the solution z of the dual problem which can be stated as: Find $z \in V$ such that

$$\rho^*(z, \varphi) = \nabla_u \rho(u, z) \varphi = \nabla_u J(u) \varphi, \quad (22)$$

for all $\varphi \in V$. Correspondingly, the finite dimensional variant has the form: Find $z_h \in V_h$ such that

$$\rho^*(z_h, \varphi) = \nabla_u J(u_h) \varphi, \quad (23)$$

for any $\varphi \in V_h$.

Assuming that the functional J is three times differentiable, the error in J can be characterized by

$$J(u) - J(u_h) = \frac{1}{2} [\rho(u_h, z - I_h z) + \rho^*(z_h, u - I_h u)] + \mathcal{R}_h, \quad (24)$$

where \mathcal{R}_h is a remainder which is cubic in $u - u_h$ and $z - z_h$ and some interpolation operator $I_h : V \rightarrow V_h$ (see Becker and Rannacher [2003] for a proof). However, the solutions u and z of the primal and dual problems are unknown in general. It is common practice to replace these unknowns by evaluable approximations $U \approx u$ and $Z \approx z$. It must be guaranteed that U and Z are not functions of the discrete space V_h (i.e. $U = u_h$ and $Z = z_h$ are not allowed), since in this case the evaluation of the residuals in Eq. (24) would vanish due to the Galerkin orthogonality. For the determination of U and Z we use a strategy based on patch-wise higher-order interpolation which is considered to be very efficient [cf. Becker and Rannacher, 2003]. Its evaluation is computationally cheap if the mesh has a so called *patch-structure*, i.e. the underlying mesh can be coarsened globally (which we will exploit in our implementation, described

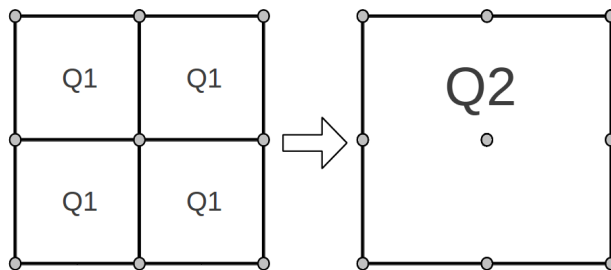


Figure 4: Patch of four cells with bi-linear finite elements form one bigger cell with bi-quadratic finite elements; the nodal points of (Lagrange) elements have identical positions.

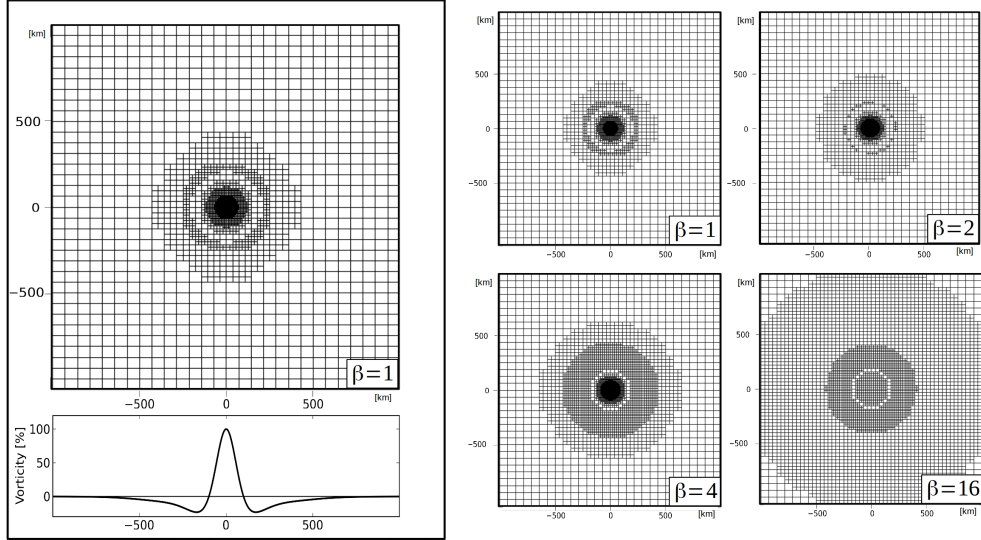


Figure 5: Adapted mesh after 6 adaptation cycles of the fixed mesh-fraction strategy (percentage of 5%) for adaptation indicators based on the enstrophy $\Phi = (\nabla \times u)^2$ with $\beta = 1$ (left), below relative vorticity values of the storm. Adapted meshes for $\beta \in \{1, 2, 4, 16\}$ (right).

later). Then, the degrees of freedom of the finite element space V_h can easily be interpreted as the degrees of freedom of a higher-order finite element space on the coarsened mesh. One simple example of this reinterpretation is shown in Fig. 4.

As described in Sect. 4.1, cell residuals R_K and jump terms R_{Γ_K} for the primal residual $\rho(u_h, Z - I_h Z)$ (restricted on cell K) can be introduced. Analogously, cell residuals R_K^* and jump terms $R_{\Gamma_K}^*$ can be introduced for the dual residual $\rho^*(z_h, U - I_h U)$. An error estimator for the error in J can be formulated in terms of these quantities:

$$|J(u) - J(u_h)| \leq \sum_{K \in \mathcal{T}_h} \eta_K, \quad (25)$$

where the so-called *error indicators* η_K are defined by

$$\eta_K := |(R_K, Z - I_h Z)_K + (R_K^*, U - I_h U)_K + (R_{\Gamma_K}, Z - I_h Z)_{\Gamma_K} + (R_{\Gamma_K}^*, U - I_h U)_{\Gamma_K}|. \quad (26)$$

Details on the generic error estimator can be found in Becker and Rannacher [2003], the specific definitions of the primal and dual problem, the cell residuals and edge terms for the time-dependent Navier-Stokes equations and its dual variant, and also an extension for evaluation of the error related to the time discretization can be found in Baumann et al. [2014].

4.3 Physically motivated criteria

Physically motivated criteria aim at the adjustment of the local mesh resolution to the solution and aim not to estimated errors. Many of these criteria refer to the smoothness of the solution by e.g. accounting for the discrete solution's gradients. In Ainsworth and Oden [2000], post-processing techniques are described that are widely used to approximate the gradient in terms of the discrete solution, i.e. $G(u_h) \approx \nabla u$. The difference between this approximation and the discrete gradient, namely $G(u_h) - \nabla u_h$, is used as an estimate for the error of the solution. Most cyclone tracking criteria that have been investigated and successfully employed in the past are based on the relative vorticity at different geopotential height levels, its gradient or curvature, cf. Hodges [1994, 1995], Murray and Simmonds [1991]. Other criteria refer to

pressure [Sinclair, 1997], geopotential height [Sinclair, 1994] and various other quantities. For an overview of methods, see Jablonowski [2004]. Although most of these criteria can easily be described qualitatively (e.g. high resolution close to a pressure minimum), their application to control the mesh refinement is in general related to a precise definition that usually requires certain thresholds or other parameters. In the following, we introduce an approach that requires only one real-valued parameter.

We denote the physical quantity based on which a criterion is defined by $\Phi = \Phi(u_h)$, e.g. the kinetic energy $\Phi(u_h) := u_h \cdot u_h$. We add an artificial h -dependency to mimic the nature of error indicators based on a posteriori error estimators, i.e. cell refinement leads to smaller indicator values. To this end, we introduce adaptation indicators ψ as composition of the cell-averaged quantity $h_K^{-d} \int_K \Phi dx$ ($d = 1, 2, 3$ is the dimension in space) and h^β ($\beta > 0$) for decreasing indication with reducing cell sizes on any cell $K \in \mathcal{T}_h$:

$$\psi_K := h_K^{\beta-d} \int_K \Phi dK. \quad (27)$$

In Fig. 5 we show the influence of the parameter β on the mesh refinement for a single vortex (defined by Eq. (5)). Here we use enstrophy $\Phi = (\nabla \times u)^2$ as the physical quantity that should be involved. The high resolution regions are localized around the area with high vorticity values. For larger values of β , the region of finer resolution is larger, but fewer levels of resolution are present. Obviously, β has a strong influence on the structure of the resulting adapted mesh, and in general it is not clear how β should be chosen. Before we apply this type of criterion to our scenario, we introduce a quality measure and solve an optimization problem in β , which is addressed in Sect. 5. For other definitions of physical criteria, as showcased by Jablonowski [2004], similar optimization problems could be formulated and solved analogously.

5 Numerical tests

We apply the different types of adaptation criteria to control the grid refinement in adaptive model runs for the binary TC interaction test case described in Sect. 3. to control mesh adaptivity. The results are compared with regard to additional costs for the evaluation of the indicators on the one hand and the quality of the solution on the other hand. The additional costs consist of computing time and storage requirements. The quality is measured in terms of the error in the final storm position of one of the storms after 96 hours, compared to the reference position $x_{ref} = (-1043.678 \text{ km}, 153.365 \text{ km})$ that has been determined with sub-grid accuracy from a high resolution reference run on a uniform mesh with 1,327,104 DOFs, which corresponds to a mesh width of approximately 10 km, i.e. ≈ 5 km distance between nodal velocity points.

The subsequent investigation adopts error indicators based on the estimators (10) and (16), goal-oriented error indicators (25), and physically motivated criteria (27). For the goal-oriented approach we consider the two goal-functionals (18) and (19). For the physically motivated indicators we investigate indicators for the enstrophy $\Phi = (\nabla \times u)^2$ and the kinetic energy $\Phi = u^2 + v^2$ as introduced in Sect. 4.3. We choose $\beta = 16$ for the enstrophy indicator and $\beta = 4$ for the energy indicator which we determined on the base of preliminary test runs that we will describe in Sect. 5.2.

5.1 Setup of the adaptive experiments

In the following, we describe how adapted meshes consisting of approx. 1,000, 2,000, 3,000, 4,000, 6,000, 8,000 and 12,000 cells are calculated for each indicator variant described before. Since a strategy is applied that is able to refine cells only (i.e. no coarsening), each adaptive run is initialized on a coarse and uniform mesh with between approx. 450 and 5,200 cells. On such initial meshes numerical simulations are conducted and the indicators are evaluated once per hour. At time $T = 96$ h, the mesh is being adapted on base of the fixed mesh-fraction strategy, which is based on a reduced indicator, defined as the cell-wise maximum indicator values over time:

$$\eta_K := \max_{i=1}^{96} \eta_{K,i} \quad \forall K \in \mathcal{T}_h. \quad (28)$$

The percentage of cells that are refined in each adaptation cycle is chosen to be 5 %. In order to guarantee that the resulting mesh fulfills the 1-irregularity condition, as introduced in Sect. 2.2, an

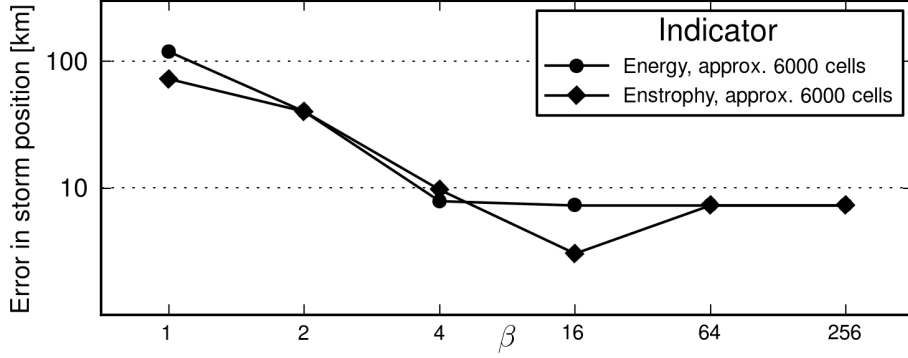


Figure 6: Error in storm position on meshes with approx. 6000 cells, adapted with an enstrophy indicator ($\Phi := (\nabla \times u)^2$, solid line) and an energy indicator ($\Phi := u^2 + v^2$, dashed line) for varying parameter β .

additional adaptation step is required in some cases. The resulting mesh may then correspond to an effective refinement percentage of more than 5%. As described in Sect. 4.2, we require a patch-structure of the mesh for the goal-oriented adaptive runs. In this case, we choose a smaller refinement percentage to result in an comparable effective increase of the number of cells. After the mesh has been adapted successfully, the first adaptation cycle is finished. On the resulting mesh the same procedure is started again, i.e. the problem is solved and the mesh is adapted. After 6 adaptation cycles, the solution's error in the storm position on the resulting mesh is analyzed.

5.2 The choice of parameter β

In Sect. 4.3, we outlined the impact of β on the adapted mesh for a simple stationary scenario with one vortex and an indicator based on the enstrophy. In this Section, we consider the scenario of two interacting cyclones. The task of finding an appropriate β can be interpreted as an optimization problem in which this parameter should be determined such that the discrete solution on the correspondingly adapted mesh has the smallest error with respect to a user-defined measure (which is the position error at time T in our application). We approximate the optimal values of β for the energy and the enstrophy indicators by sequences of adaptive numerical simulations with varying values for β on meshes with approx. 6,000 cells. The β -dependency of the corresponding position errors, that have been adapted on the base of these indicators, is shown in Fig. 6. In case of the enstrophy indicator, the minimum position error can be achieved on a mesh with $\beta = 16$. For the energy indicator, a minimum can not clearly be named: $\beta = (4, 16, 64, 256)$ lead to the same position error. To identify a good choice for β in the case of the energy indicator, we extend the optimization to a sequence of meshes with varying numbers of cells, as can be seen in Fig. 7. For $\beta = 4$ the error decreases almost monotonically with growing number of cells and for 12,000 cells the error is smaller, than for $\beta = 16$ and $\beta = 64$ (the meshes for $\beta = 16$ and $\beta = 64$ are identical²). Therefore, we choose $\beta = 4$ for the energy indicator and refrain from a fine-tuning of β which could lead to slightly better results.

²For both $\beta = 16$ and $\beta = 64$, 6 adaptation cycles lead to meshes with only two different mesh widths (h and $h/2$). Even in case of further increasing of the number of adaptation cycles, the smallest mesh width on the adapted mesh will not decrease until all cells of the initial mesh have been refined first. This can be realized when the definition of the indicators, cf. Eq. (27), is considered. Assuming a uniform mesh, a refinement of the cell with the highest indicator value on the mesh, denoted by Ψ_{\max} , leads to four cells, each having an indicator value of $(1/2)^\beta \Psi_{\max}$. Further refinement of these cells would require indicator values greater than the minimal indicator value Ψ_{\min} on the uniform mesh, $(1/2)^\beta \Psi_{\max} \geq \Psi_{\min}$. In our scenario the indicator range can be characterized on a uniform mesh by $\Psi_{\min}/\Psi_{\max} = 4.0 \cdot 10^{-4}$. Two levels of refinement would only be allowed, if $(1/2)^\beta \geq \Psi_{\min}/\Psi_{\max}$, which is not the case for $\beta \geq 12$. Hence, an increase of β beyond 12 will not affect the resulting mesh.

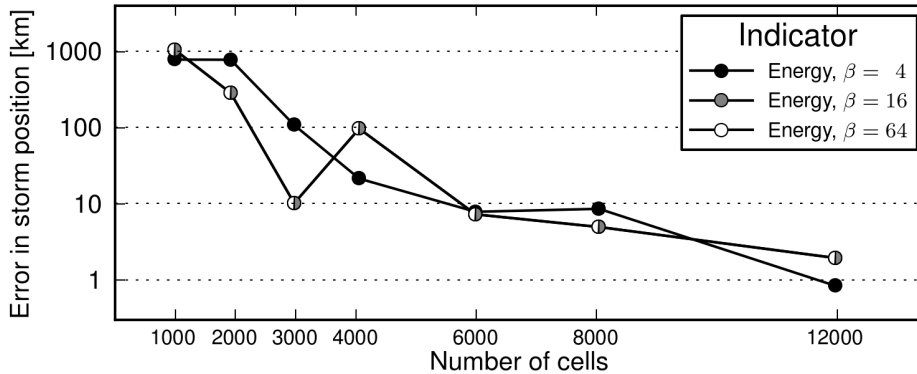


Figure 7: Error in storm position on meshes with different number of cells, adapted with an energy indicator ($\Phi := u^2 + v^2$) for varying parameter β . The choice of $\beta = 16$ and $\beta = 64$ here lead to identical meshes, which would result for all $\beta \geq 12$, see Sect. 5.2 for details.

5.3 Adapted meshes

The optimized meshes for all considered indicators are shown in Fig. 8. All indicators lead to high resolution at the area where the storm centers are located within the first 24 hours of development. Meshes resulting from the error estimators (see Figs. 8(a)–(d)) additionally feature high resolution in the area between the two storms and arms of high resolution extending to the end positions of the storms.

The energy and enstrophy indicators (cf. Figs. 8(e) – (f)) have high values close to the storms and decrease along the storm tracks. This is caused by a loss of the vortices’ intensity in time. For example, the energy loss after 96 h on an adapted mesh with about 6,000 cells accounts for approx. 56%. Therefore, mesh resolution is highest in regions where the storms are located in the first hours of development. The size of the refined areas in Figs. 8(e) – (f) is considerably larger as for the meshes adapted on base of the a posteriori indicators, see Figs. 8(a) – (d), and the finest and the coarsest mesh resolution differ in only two levels of refinement. This originates from the choice of β , whose influence on the resulting mesh structure has been discussed in Sect. 5.2.

The high resolution regions in Figs. 8(a) – (d) cover the full storm tracks. One interpretation of this is that error estimator based indicators identify the storms as most important feature at any instant in time. Furthermore, the region around the origin that lies between the two storms in the initial phase is filled with the high resolution grid. Both the instantaneous error measured in the global norm and the error in the goal functional defined at the end of the simulated time span are thus sensitive to errors in this region. It is a special property of the test case considered here, that the sensitive region according to the goal-oriented sensitivity analysis coincides with the refinement region obtained for global norms. In comparison to the meshes adapted on base of the goal-oriented approach (Figs. 8(c) – (d)), the meshes adapted on base of the error in global norms (Figs. 8(a) – (b)) show more noise in the distribution of cell sizes. This may be caused by the mesh adaptation strategy: As the goal-oriented indicators additionally require the mesh to be in a patch-structure (see 4.2), the original adaptation strategy as introduced by [Becker and Rannacher, 2003] had to be modified, so that the patch-structure is guaranteed on the resulting adapted mesh as well. To this end, it permits a refinement of patches of less than four neighboring cells.

For the vorticity goal-functional particularly high resolution can further be seen at the region of the final storms’ positions. In Fig. 8 (d) an asymmetric mesh structure relative to the storm center at final time can be identified. This is remarkable, since both the vorticity profile and the integration domain of the goal functional are symmetric. For the same scenario and goal functional, employing a differing mesh adaptation strategy led to symmetric mesh structures, [see Baumann et al., 2014]. This outlines the impact that an adaptation strategy can have.

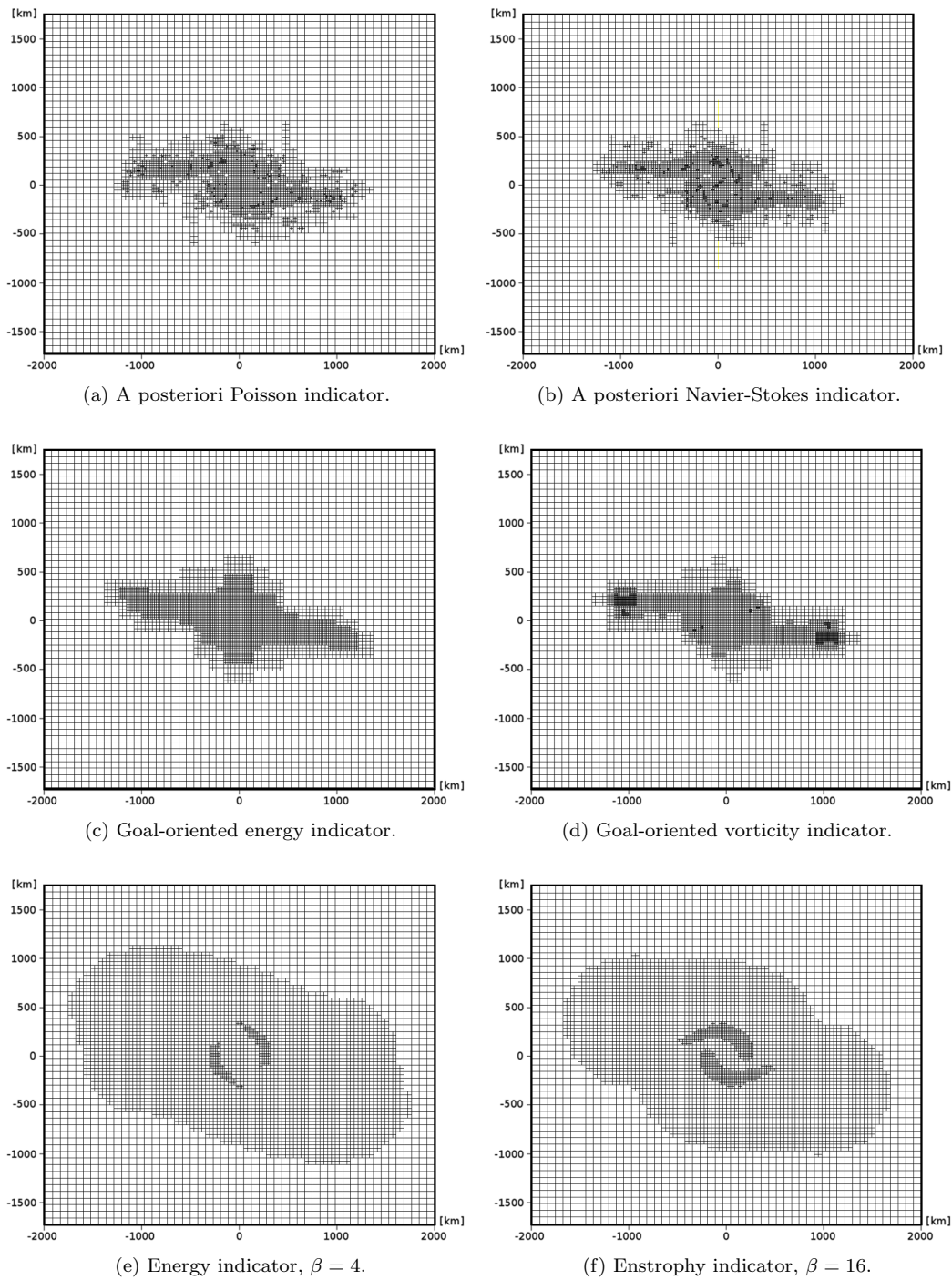


Figure 8: Adapted meshes with approx. 6,000 cells for different indicators after six adaptation cycles of the fixed mesh-fraction strategy.

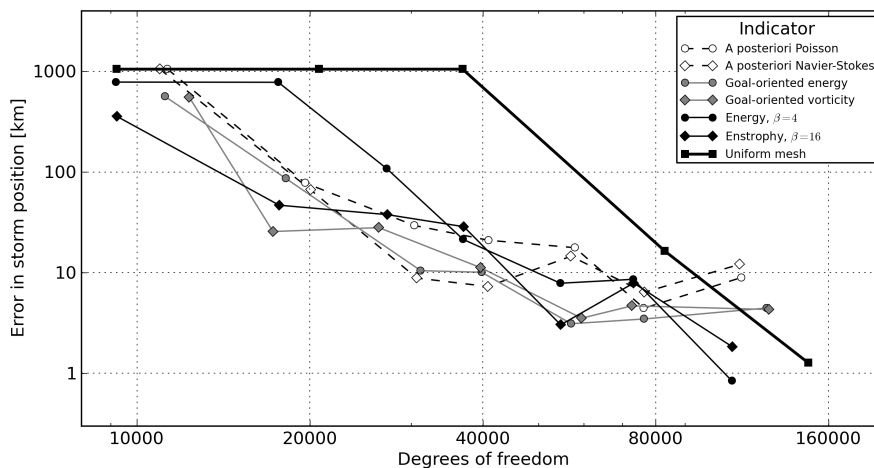


Figure 9: Error in storm position for varying number of degrees of freedom after 96 h.

5.4 Quality of the solution on adapted meshes

As a measure of the quality, we investigate the error in the final storm position of the upper left storm with the reference position x_{ref} , determined from a high resolution reference run on a uniform mesh with 1,327,104 DOFs as introduced in Sect. 5.

Figure 9 illustrates the error of numerical simulations on adapted and uniform meshes with varying problem sizes. It can clearly be seen that for problem sizes up to approximately 80,000 DOFs, all indicators lead to smaller errors than on uniform meshes. Especially for meshes with about 30,000 – 40,000 DOFs, the error in the storm position is reduced by several orders of magnitude. On uniform meshes the correct physical behavior of the two cyclones – drifting apart instead of merging – is reproduced not until problem sizes of about 40,000 DOFs. For physical indicators, already less than 10,000 DOFs are sufficient to reproduce the diverging tracks of the two storms with an error in storm position of 785 km (energy) and 357 km (enstrophy).

For problem sizes of approximately 120,000 DOFs, all indicators lead to position errors smaller than 12.5 km. Physical indicators lead to errors smaller than 2 km. As described before, we characterize the storm position as a weighted barycenter of vorticity to enable sub-grid accuracy. However, in case of varying mesh resolution close to the storm (as it is the case for meshes based on residual and goal-oriented indicators, see Fig. 8), the reliability of its determined position is limited. Small changes in the definition of the weighted barycenter can lead to a change in the determined position in the order of the local cell diameter. Therefore, small errors in the storm position could partly be caused by the post-processing procedure.

Of influential means is also the choice of the refinement strategy. Here, we used a fixed mesh-fraction strategy which only allows refinements. In Baumann [2012], numerical results of goal-oriented adaptive simulations for the same scenario and various goal-functionals but for a mesh adaptation strategy that allows also for coarsening are discussed. This strategy in combination with the considered goal-functionals defined in Eqn. (18) and Eqn. (19) leads to results that differ from those presented in Fig. 9 to some extent. In particular, all adaptive simulations resulted in position errors smaller than the error based on a simulation on a uniform mesh with the same number of cells.

5.5 Computational costs for the indicator evaluation

The determination of indicators and the adaptation of the mesh are associated with additional computational costs and memory requirements. Since we compare different adaptation criteria, we discuss the aspects of the computational costs related to the evaluation of the different indicator types introduced in Sect. 4. In order to facilitate their comparison, we do not include the costs for the numerical simulation

itself (since these are the same for all indicators) and the adaptation of the mesh (which is comparatively small).

With regard to the memory requirements, all types of indicators result in one floating point value $\eta_{K,i}$ per cell $K \in \mathcal{T}_h$ at each time step i considered. In case of the reduced indicator variant, see Eq. (28), the total storage requirement to represent all indicator information is one floating point η_K for each cell K which is being updated continuously during the iteration over time.

Since several user-dependent parameters exist that have strong influence on the overall computational costs (e.g. the frequency in which the indicators should be determined), we describe the computational complexity taking these parameters into account and additionally give the computation time of the dominating calculations (averaged time measurements, partly extrapolations). Although time measurements always depend on the specific implementation (e.g. the applied data structures) and the used hardware, they can give a rough idea of the computational costs quantitatively. In series of numerical runs on meshes with varying number of cells, it turned out that the costs for the most relevant calculations can be expressed in units of C_{Newton} (the time necessary to set up and solve one of typically three Newton steps during one time step of the primal problem) for the same mesh. For the evaluation of the three different indicator types, we introduce three parameters $f_{\text{phy}}, f_{\text{res}}, f_{\text{goal}} > 0$ to characterize the computational cost relative to C_{Newton} (e.g. $f_{\text{phy}}C_{\text{Newton}}$ describes the computing time for the evaluation of a physical indicator for one point in time).

Physical indicators of the form Eq. (27) are defined by an integral which can be evaluated by means of numerical quadrature. For some criteria, the evaluation of differential operators such as gradients, rotations or Hessians are necessary in addition. For the proposed energy and enstrophy indicators, we apply a Gauss quadrature rule with two points per dimension which is exact for the quadratic velocity elements. As described before, we specify their calculation in units of C_{Newton} for the evaluation at one point in time by $f_{\text{phy}} \cdot C_{\text{Newton}}$, where $f_{\text{phy}} = 0.07$ is a representative value for the investigated meshes. Physical indicators can be evaluated at every time step of the simulation, but evaluations based on longer time-steps can significantly reduce the computing efforts. Therefore, we introduce the parameter $N_{\text{evals}} > 0$ describing the total number of evaluations during the simulation of the scenario. Hence, the computational effort for the determination of physical indicators during one adaptation cycle amounts to

$$C_{\text{phy}} = f_{\text{phy}} \cdot C_{\text{Newton}} \cdot N_{\text{evals}}. \quad (29)$$

As described in Sect. 5.2, an additional optimization problem has to be solved to determine an appropriate value for the parameter β . The user can choose the number $N_{\text{opt}} > 0$ of optimization runs, each one related to computational costs for the preliminary simulation of the scenario on some fine grid, which is denoted by C_{prelim} . Furthermore, a reference simulation on a finer grid is needed to rate the optimization runs. This leads to additional computational costs of $C_{\text{prelim,ref}}$. The total effort for the optimization of β is therefore

$$C_{\text{phy}}^{\text{opt}} = N_{\text{opt}} \cdot C_{\text{prelim}} + C_{\text{prelim,ref}}. \quad (30)$$

In general, for each combination of physical criterion and scenario the parameter β has to be optimized. This optimization might be skipped in special situations, e.g. if the optimal value for β for the same criterion based on a related scenario is already known.

The cell and edge residuals of the residual a posteriori estimators (10) and (16) can be calculated by means of numerical quadrature. The computational cost for the quadrature in case of the cell residuals is higher than the costs for the evaluation of the two investigated physical based criteria, since second derivatives and a higher quadrature rule for exact quadrature (three Gauss points per dimension in our case) are needed. The calculation of the edge residuals take contributions of neighboring finite elements into account and leads to additional costs. Both residual type estimators were related to a computational expense of $f_{\text{res}} \cdot C_{\text{Newton}}$ at one point in time with $f_{\text{res}} = 0.91$ (averaged value). As before, the evaluations can be done at a user-defined frequency instead of at all time-steps. The total computational effort for the calculation of the indicators on a given mesh therefore results in

$$C_{\text{res}} = f_{\text{res}} \cdot C_{\text{Newton}} \cdot N_{\text{evals}}. \quad (31)$$

Excluding the optimization of β for the physical indicators, the goal-oriented approach has the highest consumption in both computing time and storage. In addition to the primal problem a dual problem has to be solved. Since the dual problem is posed backward in time and depends on the primal problem's

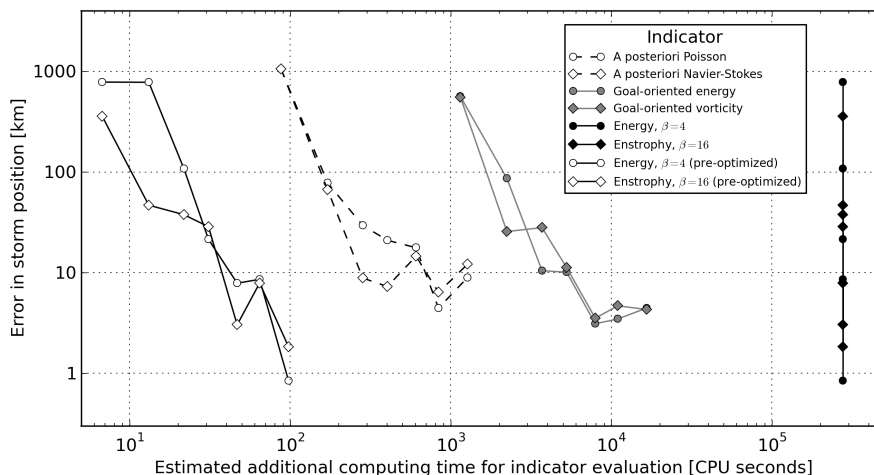


Figure 10: Error in storm position after 96 h on adapted meshes plotted over the estimated computation time for calculation of the indicators, see Eqs. (33)-(35). For the physical indicators, both the numerical costs excluding and including the optimization of β ("pre-optimized") are given. See text for details.

solution, the latter has to be stored for every point in time. The corresponding storage requirements can be enormous, but can be reduced by check-pointing approaches, which in turn will increase computing time [cf. Heuveline and Walther, 2006]. The primal and dual solutions at time t_i can be deleted once the error indicators $\eta_{K,i}$ have been determined for all cells $K \in \mathcal{T}_h$. The evaluation of the error indicators, require the evaluation of the discrete solutions in their higher-order interpretation as described in Sect. 4.2 which does not imply additional computations, but requires an adequate quadrature rule. In our case, a Gauss quadrature with four points in each dimension leads to exact quadrature. The computational costs for the evaluation of the goal-oriented indicator at one point in time is denoted by $f_{\text{goal}} \cdot C_{\text{Newton}}$, with $f_{\text{goal}} = 1.96$. As before, the user can choose the number of indicator evaluations, denoted by N_{evals} . Independent of this, the dual problem has to be solved for each time-step. Since it is linear, the required computing effort in each time step is comparable to one Newton step of the primal problem. For the scenario investigated in this article, on average four Newton steps were necessary in each time step. The additional effort to solve the dual problem thus equates to approximately one fourth of the effort to solve the primal problem. Therefore, the total computational costs for the solution of the dual problem and the determination of the estimators on a given mesh sums up to

$$C_{\text{goal}} = f_{\text{goal}} \cdot C_{\text{Newton}} \cdot N_{\text{evals}} + C_{\text{Newton}} \cdot N_{\text{tsteps}}, \quad (32)$$

assuming a time discretization with N_{tsteps} steps.

In the following, we give a quantitative comparison of the computational costs for the indicator evaluation based on Eqs. (29)-(32). Since some calculations have to be done only once (e.g. optimization of β) and others have to be done in each adaptation cycle, we investigate the additional costs of an adaptive numerical simulation consisting of several adaptation cycles. We reconsider the previously described series of adaptive numerical simulations based on the fixed mesh-fraction strategy with six adaptation loops (see Sect. 5.1) and assume the indicators to be evaluated only once per hour, i.e. $N_{\text{evals}} = 97$. Independent of the employed indicator, the adaptation strategy leads to meshes consisting of approximately equal numbers of cells. For the mesh $\mathcal{T}_{j,k}$ obtained in the j th adaptation cycle ($j = 0, \dots, 5$) towards a final mesh of approximately D_k DOFs ($k = 1, 7$ and D_k ranging from 10,000 to 120,000) we determined the averaged computation time for one Newton step, denoted by $C_{\text{Newton}}^{j,k}$. These data is included in the appendix of this article. For the optimization of β , we assume $N_{\text{opt}} = 6$ optimization runs on a uniform mesh with 150,000 DOFs (needed at minimum for this scenario, see bold line in Fig. 9) related to computational costs of $C_{\text{prelim}} = 5.1$ sec, and a high-resolution reference simulation with ten times more DOFs, related

to $C_{\text{prelim,ref}} = 60.0$ sec. All simulations include $N_{\text{tsteps}} = 1,152$ time steps. Based on the data presented in this section and in Table 1 in the appendix, the total computing time for the indicator evaluation can be approximated by

$$C_{\text{phy}}^{\text{total}} = \sum_{j=0}^5 \left(f_{\text{phy}} \cdot C_{\text{Newton}}^{j,k} \cdot N_{\text{evals}} \right) + C_{\text{phy}}^{\text{opt}}, \quad (33)$$

$$C_{\text{res}}^{\text{total}} = \sum_{j=0}^5 f_{\text{res}} \cdot C_{\text{Newton}}^{j,k} \cdot N_{\text{evals}}, \quad (34)$$

$$C_{\text{goal}}^{\text{total}} = \sum_{j=0}^5 \left(f_{\text{goal}} \cdot C_{\text{Newton}}^{j,k} \cdot N_{\text{evals}} + C_{\text{Newton}}^{j,k} \cdot N_{\text{tsteps}} \right), \quad (35)$$

for any $k = 1, \dots, 7$. The calculations on the final mesh ($j = 6$) are not considered since this mesh should not be adapted and therefore no indicators are needed.

Figure 10 illustrates the position errors resulting from the numerical simulations on the adapted meshes plotted over the approximated computing time for the evaluation of the indicators. For the physical indicators, we additionally considered the case where a pre-optimized β is assumed (hence $C_{\text{phy}}^{\text{opt}}$ is excluded). In this case, the evaluation of the physical indicators is by far the least costly: approximately one magnitude in computing time can be saved compared to a posteriori error indicators, and even two magnitudes compared to goal-oriented indicators.

The ranking changes remarkably, if the optimization of the parameter β is included. For the assumed 6 optimization runs and one additional high-resolution reference run, the computing requirements for the optimization are almost 3000 times higher than the indicator evaluations themselves. All a-posteriori error estimators cause computational costs that are up to three magnitudes lower.

6 Conclusion and Outlook

In this study several mesh adaptation methods were compared using the interaction of two idealized tropical cyclones as a test case. The position and profiles of the two storms at initial time were chosen such that the cyclones orbit each other initially and separate subsequently. Small changes in the initial distance of the storm can lead to a merger instead of a drifting apart. Besides an initial distance below a critical value, the merging of the storms can also be triggered by too coarse mesh resolution, which makes this scenario an interesting benchmark problem for adaptive methods.

We employed a mesh adaptation procedure based on the refinement of mesh cells (h-adaptivity). The selection of cells to be refined was accomplished by a fixed-fraction strategy, that was guided by different adaptation criteria, depending on cell-wise indicator values (each cell is associated with one real number). We investigated three basic approaches to define cell-wise indicators: indicators representing error contributions in global error norms, indicators representing error contributions to user-defined goal-functionals, and indicators defined in terms of physical features. We conducted series of adaptive numerical test runs based on these different indicators on seven different starting meshes and discussed the differences in terms of storm prediction quality and also the computational costs.

To quantify the quality of the solution, we estimated the error in one of the storms' final position on the adapted meshes for each indicator. Initially, we related the position error to the numerical costs for a simulation on an adapted mesh, which we measured in terms of the number of unknowns. Here, we did not account for computing costs for the evaluation of adaptation indicators or the adaptation process itself. For all adaptation criteria investigated, significant improvements in quality could be accomplished by mesh adaptation. Different than on uniform meshes, the (physically correct) drifting apart of the two storms could be reproduced on adapted meshes with approx. 20,000 unknowns for all criteria investigated. On finer meshes with approx. 120,000 unknowns, all indicators led to errors smaller than 12.5 km, with smallest errors for the physically motivated criteria. Subsequently, we related the position error to the costs for the evaluation of the different indicator values during the adaptation procedure. The computational effort was lowest for physically motivated criteria, followed by indicators based on a posteriori error estimators in global norms and highest for goal-oriented error estimators. However, the derivation of

physical indicators for physical criteria compelled an initial optimization of certain parameters, which additionally implicated significant computing efforts.

The present results demonstrate that physically motivated criteria can lead to very efficient adaptive methods, especially when measuring the efficiency in terms of the costs for the evaluation of the indicators. However, one should keep in mind that most applications will require a prior optimization of the parameter β , which can lead to enormous computational costs, deteriorating the efficiency significantly. A suboptimal choice of β can lead to inappropriate indicators (as demonstrated by the large errors in Fig. 6 for $\beta = 1, 2$, for example); in principle, even a complete failure of this criterion cannot be excluded since a fundamental connection between the solution's local characteristics and the mesh resolution does not exist in general. Nevertheless, this approach may be very efficient for certain problem types, e.g. if many similar simulations have to be carried out and only one tuning of β is sufficient.

The computational costs for the evaluation of indicators based on a posteriori error estimators for global error norms are only slightly larger compared to that of physically motivated indicators. Their definition depends on the mathematical model and not on a specific scenario (i.e. boundary and initial conditions). Hence, no additional optimization is required previously. Since error indicators based on such error estimators represent each cell's contribution to the error measured in a specific global norm, adaptive methods that equidistribute these indication tend towards a reduction of the approximation error in that norm. In many practical cases though, specific user-defined error metrics are relevant. From a mathematical point of view, adapted meshes based on a posteriori error estimators for global norms are not necessarily well-suited to improve the quality of the solution measured in the user-defined metric.

Only in the course of this study, it has turned out that the binary TC interaction scenario has a property, which works in favor of the non-goal-oriented methods. The sensitive regions for this problem are located close to the vortex tracks. Therefore, almost every point in these regions is at some instant in the considered time interval close to the vortex center and thus experiences high velocity and vorticity. Consequently, also non-goal-oriented methods are able to account for these sensitive regions. In general, however, sensitive regions are not necessarily located close to the vortex tracks. For instance, when tropical cyclones approach the mid-latitudes and experience environmental shear flow, sensitive regions for 2-day forecasts can be found several thousand kilometers away from the vortex center [Peng and Reynolds, 2006, Reynolds et al., 2010]. In an idealized study of vortices in shear flows, Scheck et al. [2013] found out that the sensitive regions are located close to streamlines connected to stagnation points in the frame moving with the vortex. These regions are characterized neither by high vorticity nor by high velocity values. From the approaches studied in this work therefore only the goal-oriented method can be expected to detect sensitive regions reliably.

While the non-goal-oriented methods may not present a general solution for the TC forecasting problem, they perform well for the test case considered in this study, require considerably less computational overhead (in case of dispensable parameter optimization), and may be well-suited for special cases. For instance, for a short-term TC forecast on timescales of hours, the sensitive regions should be located much closer to the cyclone centers [see e.g. Scheck et al., 2013, Yamaguchi et al., 2011] and thus could be refined also by the non-goal-oriented methods.

As for a posteriori error estimators in global norms, the definition of goal-oriented error estimators is generic, but problem-specific interests can be accounted for. The approach aims at minimizing the error in some user-defined goal-functional, which can represent e.g. local features (as the storm position in case of TCs). Corresponding indicators include a weighting of the local error contributions with their sensitivity to the error in the goal-functional. This sensitivity includes also the error prolongation in time (which is not the case for the alternative approaches investigated). High resolution is required only at places with prevailing influence on the goal-functional. The determination of the sensitivity information involves the solution of an additional adjoint model which can lead to a significant increase of the overall computational costs.

Several ideas exist to alleviate the biggest disadvantage of the goal-oriented approach, the computational overhead associated with the sensitivity analysis. For instance, the dual solution could be computed with lower accuracy, which would reduce the computational effort considerably. Computing optimal perturbations with lower resolution is an approach that is successfully used in operational forecast models [see e.g. Buizza et al., 2005]. A first step to investigate the feasibility of this approach has been presented in Bauer et al. [2013], who showed that grid refinement can successfully be controlled by indicators derived from error estimates for a different model based on fundamentally different numerical methods.

Future studies should investigate the adaptive methods, which we applied for a very simple scenario, for more realistic scenarios including also more complex models (e.g. 3-dimensional models). The consideration of further scenarios will allow for a more reliable rating of their efficiency, as in the scenario discussed here, the non goal-oriented indicators were leveraged by the sensitive regions being located close to the vortex tracks. Also, the potential of lowering computational efforts for the optimization by employing approaches based on reduced resolution or reduced models needs to be reviewed. In this article, we have investigated the efficiency of different adaptation criteria using the same adaptation strategy (static refinement in 6 adaptation cycles, fixed-fraction strategy, allowing only cell refinements). To address the question whether adaptive methods can outperform uniform simulations, further adaptation strategies have to be investigated. Since the overall computational costs of an adaptive method are strongly affected by the employed adaptation strategy, using a strategy that e.g. allows for coarsening or performs several coarsening or refining steps per adaptation cycle might further reduce the computational costs. Finally, for applications like the simulation of moving TCs considered in this work, dynamic mesh refinement may provide a further increase in efficiency.

Appendix

In the following, we present time measurements for setting up (i.e. assembly of the Jacobian and the residual vector) and solution of one single Newton step on different meshes, which was used to characterize the additional computing time described in Sect. 5.5. The time values represent averaged values over the adaptation cycles and the indicator types. Time measurements were made on a standard PC with an Intel(R) Core(TM) i7 processor with 2.67 GHz. For simplicity, all numerical simulations were conducted with the same parameters of the applied ILU pre-conditioned GMRES solver and based on a sequential version of our code. The parameter j denotes the adaptation step and ranges from 0 (uniform starting mesh) to 6 (final adapted mesh). The second parameter k characterizes the experiment, which is defined by the number of cells on the final adapted mesh, ranging from approx. 1,000 ($k = 1$) to approx. 12,000 ($k = 7$) cells.

j	$k = 1$	$k = 2$	$k = 3$	$k = 4$	$k = 5$	$k = 6$	$k = 7$
0	0.10	0.19	0.29	0.42	0.69	0.93	1.47
1	0.12	0.24	0.38	0.57	0.84	1.20	1.79
2	0.14	0.28	0.45	0.66	0.99	1.42	2.11
3	0.18	0.33	0.58	0.79	1.22	1.67	2.49
4	0.21	0.40	0.69	0.94	1.45	1.96	3.01
5	0.24	0.49	0.81	1.17	1.68	2.28	3.48
6	0.29	0.61	0.95	1.37	1.94	2.74	3.97

Table 1: Averaged time $C_{\text{Newton}}^{j,k}$ (in seconds) necessary to set up and solve one Newton step of the primal problem.

References

- M. Ainsworth and J. T. Oden. *A Posteriori Error Estimation in Finite Element Analysis*. John Wiley & Sons Inc., 2000.
- I. Babuka and W.C. Rheinboldt. Error estimates for adaptive finite element computation. *SIAM J. Num. Anal.*, 15:736–754, 1978.
- Wolfgang Bangerth and Rolf Rannacher. *Adaptive Finite Element Methods for Differential Equations*. Birkhäuser Verlag, 2003.

- Werner Bauer, Martin Baumann, Leonhard Scheck, Almut Gassmann, Vincent Heuveline, and Sarah Jones. Simulation of tropical-cyclone-like vortices in shallow-water icon-hex using goal-oriented r-adaptivity. *Theor. Comput. Fluid. Dyn.*, pages 1–22, 2013. ISSN 0935-4964.
- M. Baumann. *Numerical Simulation of Tropical Cyclones using Goal-Oriented Adaptivity*. PhD thesis, Karlsruhe Institute of Technology (KIT), 2012.
- M. Baumann, L. Scheck, V. Heuveline, and S.C. Jones. Goal-oriented adaptivity for idealised tropical cyclones: a binary interaction scenario. *Meteorol. Z.*, 2014. Submitted for publication.
- R. Becker and R. Rannacher. An optimal control approach to a posteriori error estimation in finite element methods. *Act. Num.*, 10:1–102, 2003.
- J. Behrens. *Adaptive Atmospheric Modeling*. Springer Verlag, Berlin, 2006.
- D. Braess. *Finite Elemente*. Springer Verlag, Berlin, 2007.
- S. Brand. Interaction of binary tropical cyclones of the western north pacific ocean. *J. Appl. Meteorol.*, 9:433–441, 1970.
- R. Buizza, P.L. Houtekamer, G. Pellerin, Z. Toth, Y. Zhu, and M. Wei. A comparison of the ecmwf, msc, and ncep global ensemble prediction systems. *Mon. Weather Rev.*, 133:1076–1097, 2005.
- K. Dong and C.J. Neumann. On the relative motion of binary tropical cyclones. *Mon. Weather Rev.*, 111:945–953, 1983.
- Kenneth Eriksson and Claes Johnson. Adaptive finite element methods for parabolic problems i: A linear model problem. *SIAM J. Num. Anal.*, 28(1):pp. 43–77, 1991. ISSN 00361429.
- S. Fujiwhara. On the growth and decay of vortical systems. *Quart. J. Roy. Meteor. Soc.*, 49:75–104, 1923.
- V. Girault and P.-A. Raviart. *Finite element methods for Navier-Stokes equations : theory and algorithms*. Springer series in computational mathematics ; 5. Springer, Berlin, 1986.
- M. D. Gunzburger. *Finite Element Methods for Viscous Incompressible Flows*. Academic Press, 1989.
- V. Heuveline. Hiflow3 - a flexible and hardware-aware parallel finite element package. In *Proceedings of the 9th Workshop on Parallel/High-Performance Object-Oriented Scientific Computing of POOSC '10*. ACM, New York, NY, USA, 2010.
- V. Heuveline and R. Rannacher. Duality-based adaptivity in the hp-finite element method. *J. Numer. Math.*, 11:95–113, 2003.
- V. Heuveline and F. Schieweck. On the inf-sup condition for higher order mixed fem on meshes with hanging nodes. *ESAIM: Math. Modell. Numer. Anal.*, 41(1):1–20, 4 2007.
- Vincent Heuveline and Andrea Walther. Online checkpointing for parallel adjoint computation in pdes: Application to goal-oriented adaptivity and flow control. In *Euro-Par 2006 Parallel Processing*, volume 4128 of *Lecture Notes in Computer Science*, pages 689–699. Springer Berlin Heidelberg, 2006.
- K. I. Hodges. A general method for tracking analysis and its application to meteorological data. *Mon. Weather Rev.*, 122:2573 – 2586, 1994.
- K. I. Hodges. Feature tracking on the unit sphere. *Mon. Weather Rev.*, 123:3458 – 3465, 1995.
- G.J. Holland and G.S. Dietachmayer. On the interaction of tropical-cyclone-scale vortices. iii. continuous barotropic vortices. *Quart. J. Roy. Meteor. Soc.*, 119:1381–1398, 1993.
- Weizhang Huang and Robert D. Russell. *Adaptive moving mesh methods*. Applied mathematical sciences. Springer, New York, Heidelberg, London, 2011. ISBN 978-1-4419-7915-5. URL <http://opac.inria.fr/record=b1134245>.

- C. Jablonowski. *Adaptive grids in weather and climate modeling*. PhD thesis, The University of Michigan, 2004.
- M. V. Melander, N. J. Zabusky, and J. C. McWilliams. Symmetric vortex merger in two dimensions: causes and conditions. *J. Fluid Mech.*, 195:303–340, 1988.
- R. J. Murray and I. Simmonds. A numerical scheme for tracking cyclone centers from digital data. part i: Development and operation of the scheme. *Austr. Meteorol. Mag.*, 39:155 – 166, 1991.
- M. S. Peng and C. A. Reynolds. Sensitivity of tropical cyclone forecasts as revealed by singular vectors. *J. Atmos. Sci.*, 63:2508–2528, 2006.
- A. Quarteroni and A. Valli. *Numerical approximation of partial differential equations*. Springer series in computational mathematics; 23. Springer, Berlin, 1994.
- Carolyn A. Reynolds, James D. Doyle, Richard M. Hodur, and Jin Hao. Naval research laboratory multiscale targeting guidance for t-parc and tcs-08. *Wea. Forecasting*, 25(2):526 – 544, 2010.
- E. A. Ritchie and G. J. Holland. On the interaction of tropical-cyclone scale vortices. ii: Interacting vortex patches. *Quart. J. Roy. Meteor. Soc.*, 119:1363–1379, 1993.
- L. Scheck, S. C. Jones, and M. Jukes. The resonant interaction of a tropical cyclone and a tropopause front in a barotropic model, part i: Zonally-oriented front. *J. Atmos. Sci.*, 68:405–419, 2011.
- Leonhard Scheck, Sarah C Jones, and Vincent Heuveline. Singular vectors for barotropic, hurricane-like vortices in horizontal shear: Structure and perturbation growth mechanisms. *Journal of the Atmospheric Sciences*, (2013), 2013.
- F. Schieweck. A-stable discontinuous galerkin-petrov time discretization of higher order. *J. Numer. Math.*, 18:25–57, 2010.
- Michael Schmich. *Adaptive Finite Element Methods for Computing Nonstationary Incompressible Flows*. PhD thesis, University of Heidelberg, 2009.
- M. R. Sinclair. An objective cyclone climatology for the southern hemisphere. *Mon. Weather Rev.*, 122: 2239–2256, 1994.
- M. R. Sinclair. Objective identification of cyclones and their circulation intensity, and climatology. *Wea. Forecasting*, 12:595–612, 1997.
- R. K. Smith, W. Ulrich, and G. Dietachmayer. A numerical study of tropical cyclone motion using a barotropic model. i: The role of vortex asymmetries. *Quart. J. Roy. Meteor. Soc.*, 116(492):337–362, 1990.
- R. Temam. *Navier-Stokes equations and nonlinear functional analysis*. Regional conference series in applied mathematics; 66. Soc. for Industrial and Applied Mathematics, Philadelphia, 2. ed. edition, 1995.
- R. Verfürth. A posteriori error estimators for the stokes equations. *Numerische Mathematik*, 55:309–325, 1989.
- R. Verfürth and W. Hackbusch. A posteriori error estimators and adaptive mesh-refinement for a mixed finite element discretization of the navier-stokes equations. In *Numerical Treatment of the Navier-Stokes Equations, Proceedings of the 5th GAMM-Seminar, Kiel, Jan. 1989*, volume 30, pages 145–152. Vieweg, Braunschweig, 1990.
- H. Weller, T. Ringler, M. Piggott, and N. Wood. Challenges facing adaptive mesh modeling of the atmosphere and ocean. *Bull. Am. Meteorol. Soc.*, 91:105–108, 2010.
- M. Yamaguchi, D.S. Nolan, M. Iskandarani, S.J. Majumdar, and C.A. Peng M.S., Reynolds. Singular vectors for tropical cyclonelike vortices in a nondivergent barotropic framework. *J. Atmos. Sci.*, 68: 2273–2291, 2011.

Preprint Series of the Engineering Mathematics and Computing Lab

recent issues

- No. 2014-02 Nicolai Schoch, Christoph Paulus, Stefan Suwelack, Stefanie Speidel, Rüdiger Dillmann, Vincent Heuveline: Simulation of Complex Cuts in Soft Tissue with the Extended Finite Element Method (X-FEM)
- No. 2014-01 Martin Wlotzka, Vincent Heuveline: A parallel solution scheme for multiphysics evolution problems using OpenPALM
- No. 2013-02 Nicolai Schoch, Stefan Suwelack, Rüdiger Dillmann, Vincent Heuveline: Simulation of Surgical Cutting in Soft Tissue using the Extended Finite Element Method (X-FEM)
- No. 2013-01 Martin Schindewolf, Björn Rocker, Wolfgang Karl, Vincent Heuveline: Evaluation of two Formulations of the Conjugate Gradients Method with Transactional Memory
- No. 2012-07 Andreas Helfrich-Schkarbanenko, Vincent Heuveline, Roman Reiner, Sebastian Ritterbusch: Bandwidth-Efficient Parallel Visualization for Mobile Devices
- No. 2012-06 Thomas Henn, Vincent Heuveline, Mathias J. Krause, Sebastian Ritterbusch: Aortic Coarctation simulation based on the Lattice Boltzmann method: benchmark results
- No. 2012-05 Vincent Heuveline, Eva Ketelaer, Staffan Ronnas, Mareike Schmidtobreck, Martin Wlotzka: Scalability Study of HiFlow³ based on a Fluid Flow Channel Benchmark
- No. 2012-04 Hartwig Anzt, Armen Beglarian, Suren Chilingaryan, Andrew Ferrone, Vincent Heuveline, Andreas Kopmann: A unified Energy Footprint for Simulation Software
- No. 2012-03 Vincent Heuveline, Chandramowli Subramanian: The Coffee-table Book of Pseudospectra
- No. 2012-02 Dominik P.J. Barz, Hendryk Bockelmann, Vincent Heuveline: Electrokinetic optimization of a micromixer for lab-on-chip applications
- No. 2012-01 Sven Janko, Björn Rocker, Martin Schindewolf, Vincent Heuveline, Wolfgang Karl: Software Transactional Memory, OpenMP and Pthread implementations of the Conjugate Gradients Method - a Preliminary Evaluation
- No. 2011-17 Hartwig Anzt, Jack Dongarra, Vincent Heuveline, Piotr Luszczek: GPU-Accelerated Asynchronous Error Correction for Mixed Precision Iterative Refinement
- No. 2011-16 Vincent Heuveline, Sebastian Ritterbusch, Staffan Ronnås: Augmented Reality for Urban Simulation Visualization
- No. 2011-15 Hartwig Anzt, Jack Dongarra, Mark Gates, Stanimire Tomov: Block-asynchronous multigrid smoothers for GPU-accelerated systems
- No. 2011-14 Hartwig Anzt, Jack Dongarra, Vincent Heuveline, Stanimire Tomov: A Block-Asynchronous Relaxation Method for Graphics Processing Units
- No. 2011-13 Vincent Heuveline, Wolfgang Karl, Fabian Nowak, Mareike Schmidtobreck, Florian Wilhelm: Employing a High-Level Language for Porting Numerical Applications to Reconfigurable Hardware

Preprint Series of the Engineering Mathematics and Computing Lab (EMCL)

